Dentomaxillofacial Radiology (2013) 42, 20120265

http://dmfr.birjournals.org

RESEARCH

Diagnostic value of MRI for odontogenic tumours

M Fujita[1], H Matsuzaki[2], Y Yanagi[2], M Hara[1], N Katase[3], M Hisatomi[1], T Unetsubo[1], H Konouchi[2], H Nagatsuka[3] and J-I Asaumi*[,1,2]

[1]*Department of Oral and Maxillofacial Radiology, Okayama University Graduate School of Medicine, Dentistry and Pharmaceutical Sciences, Okayama, Japan;* [2]*Department of Oral Diagnosis and Dentomaxillofacial Radiology, Okayama University Hospital, Okayama, Japan;* [3]*Department of Oral Pathology and Medicine, Okayama University Graduate School of Medicine, Dentistry and Pharmaceutical Sciences, Okayama, Japan*

Objectives: To evaluate the diagnostic value of MRI for odontogenic tumours.
Materials and methods: 51 patients with odontogenic tumours were subjected to pre-operative MRI examinations. For tumours with liquid components, *i.e.* ameloblastomas and keratocystic odontogenic tumours (KCOTs), the signal intensity (SI) uniformity of their cystic components ($U\Sigma$) was calculated and then their $U\Sigma$ values were compared. For tumours with solid components that had been examined using dynamic contrast-enhanced MRI (DCE-MRI), their CI_{max} (maximum contrast index), T_{max} (the time when CI_{max} occurred), CI_{peak} ($CI_{max} \times 0.90$), T_{peak} (the time when CI_{peak} occurred) and CI_{300} (*i.e.* the CI observed at 300 s after contrast medium injection) values were determined from CI curves. We then classified the odontogenic tumours according to their DCE-MRI parameters.
Results: Significant differences between the $U\Sigma$ values of the ameloblastomas and KCOT were observed on T_1 weighted images, T_2 weighted images and short TI inversion recovery images. Depending on their DCE-MRI parameters, we classified the odontogenic tumours into the following five types: Type A, $CI_{peak} > 2.0$ and $T_{peak} < 200$ s; Type B, $CI_{peak} < 2.0$ and $T_{peak} < 200$ s; Type C, $CI_{300} > 2.0$ and $T_{max} < 600$ s; Type D, $CI_{300} > 2.0$ and $T_{max} > 600$ s; Type E, $CI_{300} < 2.0$ and $T_{max} > 600$ s.
Conclusion: Cystic component SI uniformity was found to be useful for differentiating between ameloblastomas and KCOT. However, the DCE-MRI parameters of odontogenic tumours, except for odontogenic fibromas and odontogenic myxomas, contributed little to their differential diagnosis.
Dentomaxillofacial Radiology (2013) **42,** 20120265. doi: 10.1259/dmfr.20120265

Cite this article as: Fujita M, Matsuzaki H, Yanagi Y, Hara M, Katase N, Hisatomi M, et al. Diagnostic value of MRI for odontogenic tumours. *Dentomaxillofac Radiol* 2013; **42:** 20120265.

Keywords: odontogenic tumour; magnetic resonance imaging; ameloblastoma; keratocystic odontogenic tumour

Introduction

Odontogenic tumours are neoplasms derived from the epithelial, ectomesenchymal and/or mesenchymal elements of the tooth-forming apparatus and account for between 1.0% and 3.0% of all oral lesions.[1–3] There are many histopathological types of odontogenic tumour, approximately 97% of which are benign, and the frequencies of each odontogenic tumour vary according to racial and geographical differences.[1–4] Odontogenic tumours usually occur intraosseously within the jawbones, while extraosseous tumours nearly always occur in the tooth-bearing mucosa.[1] The clinical features of most benign odontogenic tumours are non-specific, *i.e.* slow expansive growth with or without slight pain. On the other hand, the most common symptom of malignant odontogenic tumour is pain followed by rapid swelling. On radiographs, odontogenic tumours appear

*Correspondence to: Dr J-I Asaumi, Department of Oral and Maxillofacial Radiology, Field of Tumor Biology, Okayama University Graduate School of Medicine, Dentistry and Pharmaceutical Sciences, 5-1, Shikata-cho, 2-Chome, Kita-ku, Okayama City, Okayama 700-8558, Japan. E-mail: asaumi@md.okayama-u.ac.jp
Received 25 July 2012; revised 6 September 2012; accepted 20 September 2012

radiolucent and/or radio-opaque depending on the amounts of soft and/or hard tissue that they contain.[1]

In the radiological diagnosis of jawbone lesions, odontogenic tumours with hard-tissue components are relatively easy to distinguish from cystic lesions because they display more characteristic radiographic findings than odontogenic tumours without hard-tissue components and jawbone cysts. Odontoma, a type of hamartoma, is an odontogenic tumour that contains hard-tissue components, and, on radiographs, it usually appears as a radio-opaque area, which occupies the majority of the lesion, surrounded by a single radiolucent layer.[1] Conversely, other odontogenic tumours with hard-tissue components, *e.g.* adenomatoid odontogenic tumour (AOT), calcifying cystic odontogenic tumour (CCOT) and calcifying epithelial odontogenic tumour, are detected as radiolucent lesions with radio-opaque foci. Although the latter tumours often display a similar appearance on radiographs, they are rare.[2–4] On the other hand, some of these tumours do not display any radio-opaque foci on radiographs, and odontogenic tumours with large soft-tissue components can also display similar findings.[1] Therefore, it is difficult for radiologists to distinguish between odontogenic tumours with radiolucent areas, which frequently occur in the jawbones.

MRI, which possesses superior soft-tissue contrast, is a useful imaging modality for diagnosing tumours with soft-tissue components. Some authors, including us, have previously reported the usefulness of MRI, including dynamic contrast-enhanced MRI (DCE-MRI), for the differential diagnosis of odontogenic tumours.[5–12] However, these previous studies were case reports or comparison studies involving one or a few histopathological types.[5–12] Therefore, the aims of this study were to evaluate the diagnostic value of MRI including DCE-MRI for odontogenic tumours and to establish criteria for their diagnosis.

Materials and methods

Patients

51 patients who underwent MRI examinations at our hospital between April 1998 and November 2011 and were histopathologically diagnosed with odontogenic tumours, which were classified according to the World Health Organization (WHO) classification (2005), were enrolled in this study.[1] The subjects included 24 males and 27 females (mean age, 34.5 years; range, 11–75 years). All patients were examined with an identical MRI device. The study protocol was approved by our institutional review board (no. 232). Information about the odontogenic tumours is shown in Table 1. The patients' histopathological diagnoses included 49 benign tumours [26 ameloblastomas, 14 keratocystic odontogenic tumours (KCOTs), 4 odontogenic myxomas, 2 odontogenic fibromas and 3 AOTs] and 2 malignant tumours [1 ameloblastic carcinoma and 1 primary intraosseous squamous cell carcinoma (PIOSCC)]. The ameloblastomas were histologically classified as follows: 20 lesions were classified as the solid/multicystic type, 2 lesions belonged to the desmoplastic type and 4 lesions were categorized as the unicystic type. The tumour locations of all subjects were as follows: 15 lesions were located in the maxilla and 36 lesions were found in the mandible (Table 1).

Table 1 Histopathological diagnosis and tumour locations of odontogenic tumours

	Tumour location	
Histopathological diagnosis	*Maxilla (n = 15)*	*Mandible (n = 36)*
Benign		
Ameloblastoma ($n = 26$)	6	20
Keratocystic odontogenic tumour ($n = 14$)	6	8
Odontogenic myxoma ($n = 4$)	2	2
AOT ($n = 3$)	0	3
Odontogenic fibroma ($n = 2$)	0	2
Malignant		
Ameloblastic carcinoma ($n = 1$)	1	0
PIOSCC ($n = 1$)	0	1

AOT, adenomatoid odontogenic tumour; PIOSCC, primary intraosseous squamous cell carcinoma.

MRI protocol

The MRI examinations were performed using a 1.5 T unit (Magnetom Vision; Siemens, Erlangen, Germany) with a head or head and neck coil. In all cases, T_1 weighted images (T_1WIs) were acquired with a spin-echo sequence using repetition time (TR)/echo time (TE) parameters of 450–705/10–15 ms. In addition, T_2 weighted images (T_2WIs) with fat suppression were acquired for 26 cases using a turbo-spin echo sequence and TR/TE parameters of 2400–4200/90–105 ms and short TI inversion recovery (STIR) images were obtained for 28 cases using a turbo-spin echo sequence and TR/TE/inversion time (TI) parameters of 3476–7268/60–140 ms. Images were taken in both the axial and the coronal planes.

In 43 cases, we performed DCE-MRI under the conditions described below. The DCE-MRI were acquired via three-dimensional fast imaging with a steady-state precession sequence using the following parameters: TR, 5 ms; TE, 2 ms; flip angle, 25°; 16 partitions in a 48 mm slab, resulting in an effective thickness of 3 mm and a 250 × 188 mm rectangular field of view and a 256 × 192 matrix, resulting in a 0.98×0.98 mm pixel size. The first series of DCE-MRI was composed of 21 consecutive scans for 18 cases, 20 consecutive scans for 4 cases and 14 consecutive scans for 21 cases. The acquisition time for each scan was 14 s, and the inter-scan interval was 1 s, resulting in total scan times of 300, 210 and 195 s, respectively. Before the second scan, 0.2 ml kg^{-1} of contrast medium was administered intravenously for 6 s at a rate of approximately 2.0 ml s^{-1} via manual injection. We used two types of contrast medium, gadopentetate dimeglumine (Magnevist®; Nihon

Schering, Osaka, Japan) and gadodiamide hydrate (Omniscan; Daiichi Sankyo, Tokyo, Japan).

Delayed series of DCE-MRI were acquired during the period from approximately 700 to 1100 s. Two consecutive scans were performed for the delayed series of DCE-MRI, resulting in a total scan time of 30 s. Contrast-enhanced (CE) T_1WIs were acquired after the acquisition of the first series of DCE-MRI and before the delayed series of DCE-MRI scans.

Analysis of the signal intensity uniformity of the tumours' cystic components

We analysed the signal intensities (SIs) of the cystic components of odontogenic tumours. In this analysis, we selected lesions with cystic components whose minor diameter was greater than 5 mm to ensure the accuracy of the data. We performed the following evaluations in 33 patients whose lesions displayed cystic components on MR images. To quantitatively assess the tumours' cystic components, we evaluated the uniformity of each tumour's cystic component SI using the abovementioned sequences. In this analysis, the patients' histopathological diagnoses included 19 ameloblastomas (solid/multicystic type, 14 lesions; desmoplastic type, 1 lesion; unicystic type, 4 lesions) and 14 KCOTs. A region of interest (ROI) was drawn manually on CE T_1WIs so that it included the region in which the diameter of the cystic component was greatest and avoided the enhanced peripheral zone (Figure 1). The ROI was then copied from the CE T_1WI to the T_1WI, T_2WI and/or STIR images.

To evaluate the uniformity of the SI of each lesion's cystic components, the maximum SI (S_{max}) and minimum SI (S_{min}) of the ROIs on T_1WIs (33 cases), T_2WIs (18 cases) and/or STIR images (17 cases) were calculated for each lesion using a workstation (Synapse Vincent; Fujifilm Medical Co., Tokyo, Japan). We then used the formula developed by the American Association of Physicists in Medicine to calculate uniformity ($U\Sigma$) values for each lesion, *i.e.* $U\Sigma\ (\%) = 100 \times [1 - (S_{max} - S_{min})/(S_{max} + S_{min})]$.[13]

Analysis of DCE-MRI parameters

In this analysis, we selected lesions with solid components whose minor diameter was greater than 5 mm to ensure the accuracy of the data. Thus, we evaluated the records of 27 patients in this analysis. The patients' histopathological diagnoses included 16 ameloblastomas (solid/multicystic type, 13 lesions; desmoplastic type, 2 lesions; unicystic type, 1 lesion), 4 odontogenic myxomas, 3 AOTs, 2 odontogenic fibromas, 1 ameloblastic carcinoma and 1 PIOSCC. The ROI was drawn so that it included the region in which the diameter of the tumour was greatest and avoided the vessels and cystic parts of the tumour (Figure 2). The mean SI of the ROI was calculated for each lesion using a workstation. The contrast index (CI) was calculated using the formula CI = [SI (post-contrast) – SI (pre-contrast)]/SI (pre-contrast). The time course of the CI was then plotted to obtain a CI curve. The parameters derived from the CI curves were maximum CI (CI_{max}), *i.e.* the maximum amplitude of contrast enhancement, and T_{max}, *i.e.* the time at which CI_{max} occurred. We then calculated CI_{peak}, which was defined as the first CI measurement that satisfied $CI_{max} \times 0.90$, and T_{peak}, which was the time at which CI_{peak} occurred. Furthermore, we also calculated the CI_{300} value, *i.e.* the CI observed at 300 s after the contrast medium injection. T_{peak} and CI_{300} were calculated from the curve using linear interpolation

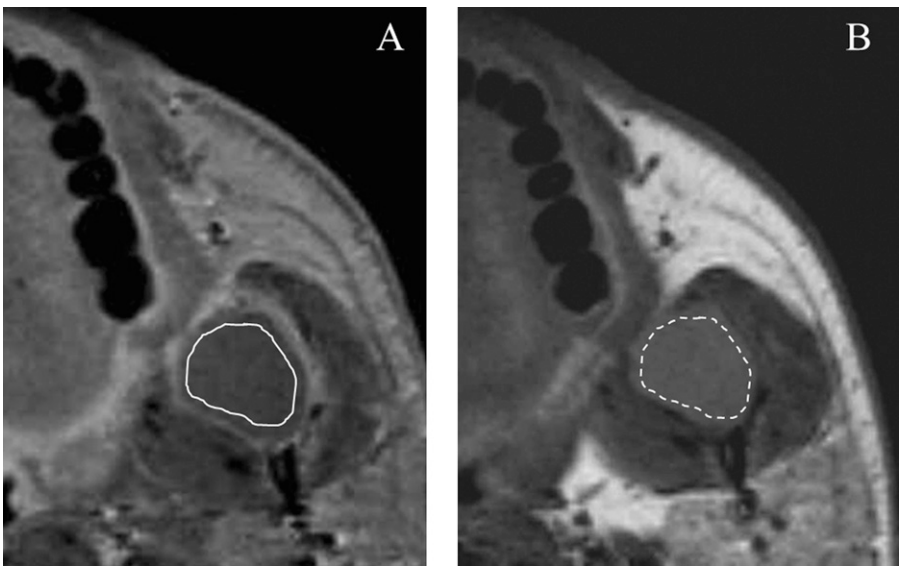

Figure 1 Ameloblastoma of the left mandibular ramus in a 41-year-old male. (a) The region of interest (ROI; solid line), which avoided the enhanced peripheral zone, was drawn on a transverse contrast-enhanced (CE) T_1 weighted image (T_1WI). (b) The ROI (dashed line) was then copied from the CE T_1WI to the corresponding T_1WI

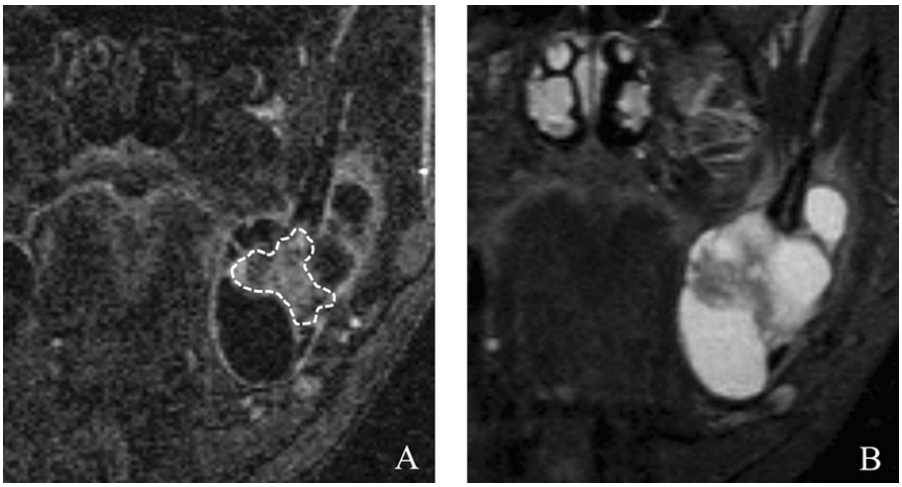

Figure 2 Ameloblastoma extending from the left mandible to the ramus in a 42-year-old male. (a) The region of interest (dashed line), which avoided the cystic parts of the tumour, was marked on a coronal dynamic image. (b) The corresponding short TI inversion recovery image

as described below. The linear-interpolation calculation was performed using the following formula:

$$y = ya + (yb - ya)/(xb - xa) \times (x - xa)$$

where y is the CI to be obtained, x is the time to be obtained, (x, y) is the point to be obtained between point A and point B, point A = (xa, ya), point B = (xb, yb) and $xa \leq x \leq xb$. The CI curve parameters are summarised in Figure 3.

Then, we tried to classify the odontogenic tumours based on their DCE-MRI parameters.

Statistical analysis of cystic component uniformity ($U\Sigma$)
We compared the cystic component uniformity ($U\Sigma$) values obtained with each sequence between ameloblastomas and KCOTs. We used the Mann–Whitney U-test for comparisons between each value. Furthermore, receiver operating characteristic (ROC) analysis was used to assess the optimal uniformity cutoff value points for differentiating between ameloblastomas and KCOTs, *i.e.* the cutoff values that provided the best combination of sensitivity and specificity. Thus, the optimal cutoff value was defined as the value that corresponded to the maximum sum of sensitivity and specificity. Fitted ROC curves were constructed with data analysis software. All statistical analyses were performed with the JMP 9 software (SAS Institute, Cary, NC). p-values of <0.05 were considered significant.

Results

Analysis of cystic component uniformity
Regarding cystic component uniformity ($U\Sigma$), significant differences between the $U\Sigma$ values of the ameloblastomas and KCOTs were observed on T_1WIs ($p < 0.05$), T_2WIs

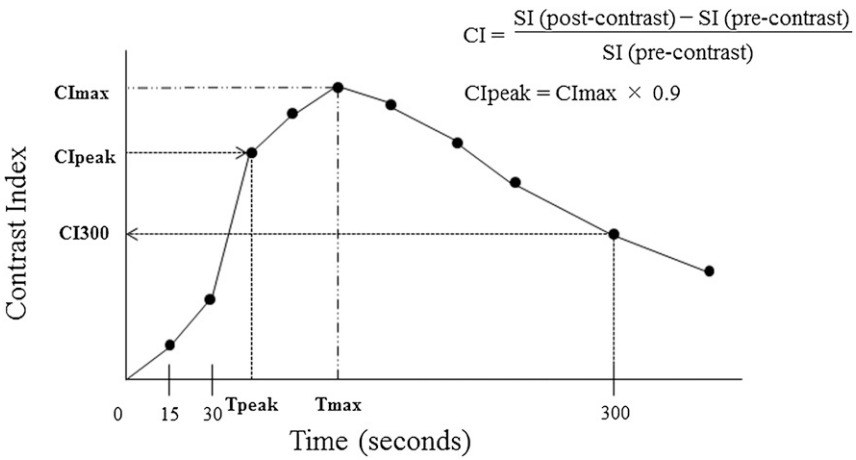

Figure 3 Contrast index (CI) curves constructed using dynamic contrast-enhanced MRI and CI curve parameters. The CI_{300} represents the CI observed at 300 s after the contrast medium injection. CI_{max}, maximum contrast index; CI_{peak}, $CI_{max} \times 0.90$; SI, signal intensity; T_{max}, the time when CI_{max} occurred; T_{peak}, the time when CI_{peak} occurred

Table 2 Receiver operating characteristic (ROC) analysis of uniformity of T_1 weighted images (T_1WIs), T_2 weighted images (T_2WIs) and short tau inversion–recovery (STIR) images for discrimination between ameloblastomas and keratocystic odontogenic tumours

Imaging sequences	*Cutoff value (%)*	*AUC*	*Sensitivity (%)*	*Specificity (%)*	*Accuracy (%)*
T_1WI	75.7	0.868	78.9	85.7	81.8
T_2WI	82.4	1.000	100	100	100
STIR image	73.5	0.971	100	85.7	94.1

AUC, area under the ROC curve.

($p < 0.05$) and STIR images ($p < 0.05$). The results of our ROC analysis of the utility of $U\Sigma$ values for differentiating between ameloblastoma and KCOTs are shown in Table 2. After considering the best combination of sensitivity, specificity and accuracy, we selected 75.7% (accuracy 81.8%) for T_1WIs, 82.4% (accuracy 100%) for T_2WIs and 73.5% (accuracy 94.1%) for STIR images as the optimal $U\Sigma$ cutoff values for differentiating between ameloblastomas and KCOTs.

Analysis of DCE-MRI parameters

The relationships between T_{max} and CI_{max} in the cases subjected to the DCE-MRI parameter analysis are shown in Figure 4. From these results, the odontogenic tumours were divided into two groups according to their T_{max} values: the early enhancement group, which displayed T_{max} values of less than 300 s, and the late enhancement group, which demonstrated T_{max} values of more than 300 s. The early enhancement group consisted of 12 ameloblastomas, 2 AOTs, 1 ameloblastic carcinoma and 1 PIOSCC. On the other hand, the late enhancement group was composed of four ameloblastomas, two odontogenic fibromas, four odontogenic myxomas and one AOT.

The relationship between T_{peak} and CI_{peak} values of the early enhancement group is shown in Figure 5. Using these results, we further categorized the early enhancement group into two groups according to their CI_{peak} values: one group displayed CI_{peak} values of more than 2.0, while the other group demonstrated CI_{peak} values of less than 2.0. In addition, the relationship between T_{max} and CI_{300} in the late enhancement group is shown in Figure 6. We further categorized the late enhancement group into three groups according to their T_{max} and CI_{300} values: one group displayed CI_{300} values of more than 2.0 and T_{max} values of less than 600 s, the second group demonstrated CI_{300} values of more than 2.0 and T_{max} values of more than 600 s and the third group displayed CI_{300} values of less than 1.0 and T_{max} values of more than 600 s.

Finally, we classified the odontogenic tumours into five types (Types A–E) according to the features of their CI curves (Figure 7). We defined the five CI curve types as follows: Type A, early peak and strong enhancement (CI_{peak} more than 2.0 and T_{peak} less than 200 s); Type B, early peak and weak enhancement (CI_{peak} less than 2.0 and T_{peak} less than 200 s); Type C, gradual strong enhancement with washout (CI_{300} more than 2.0 and T_{max} less than 600 s); Type D, gradual strong enhancement without washout (CI_{300} more than 2.0 and T_{max} more than 600 s); Type E, gradual weak

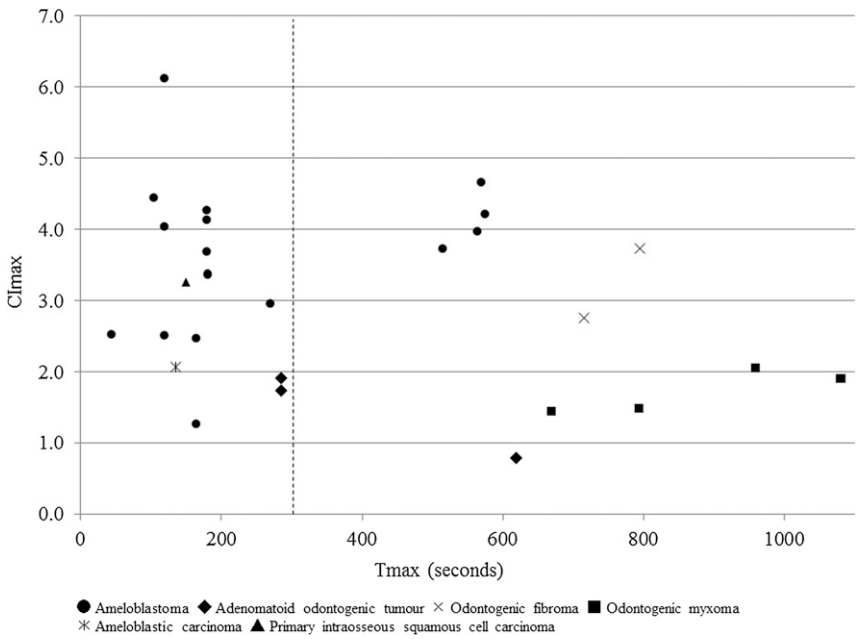

Figure 4 The relationship between the time when the maximum contrast index (CI_{max}) occurred (T_{max}) and the CI_{max} values of the 27 cases subjected to the dynamic contrast-enhanced MRI parameter analysis. The odontogenic tumours were divided into two groups according to their T_{max} values (vertical dashed line: cutoff point).

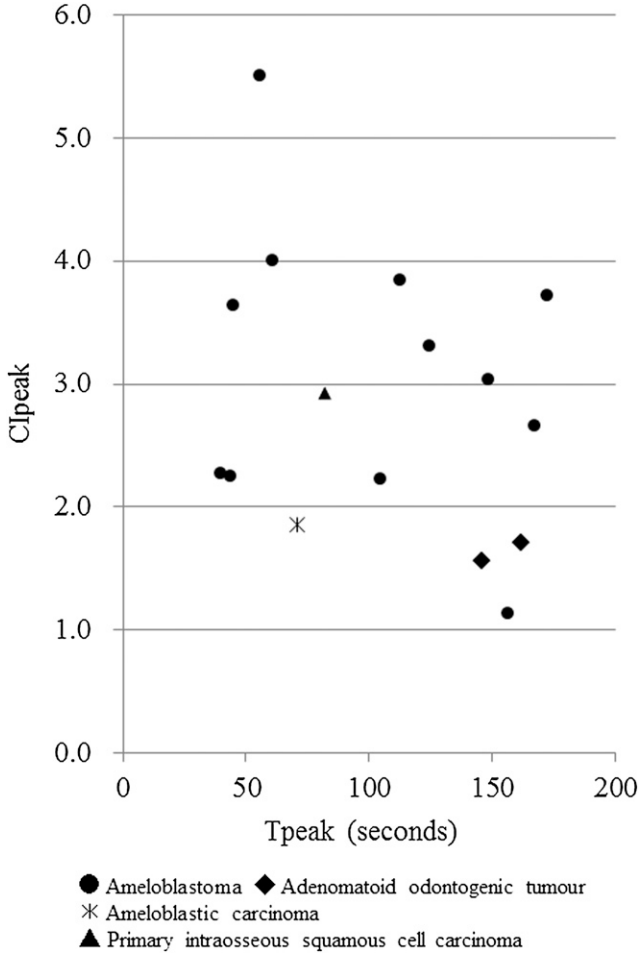

Figure 5 The relationship between the time when the CI_{peak} [*i.e.* maximum contrast injection (CI_{max}) × 0.90] occurred (T_{peak}) and the CI_{peak} values of the odontogenic tumours in the early enhancement group [time when CI_{max} occurred (T_{max}) < 300 s].

enhancement without washout (CI_{300} less than 2.0 and T_{max} more than 600 s). Table 3 shows the results of our CI curve classification. All the ameloblastomas were categorized as Type A, B or C, and two-thirds of them were classified as Type A. The AOTs were classified into Types A and E, whereas the odontogenic myxomas and odontogenic fibromas were categorized as Types D and E, respectively. The two malignant odontogenic tumours (the ameloblastic carcinoma and PIOSCC) were classified as Types B and A, respectively.

Regarding the ameloblastoma that constituted the majority in this study, the distributions of tumour locations and histological types of ameloblastoma among each CI curve type are shown in Figure 8.

Discussion

In this retrospective study, we evaluated the utility of MRI for diagnosing odontogenic tumours that are mainly composed of soft-tissue components, which are

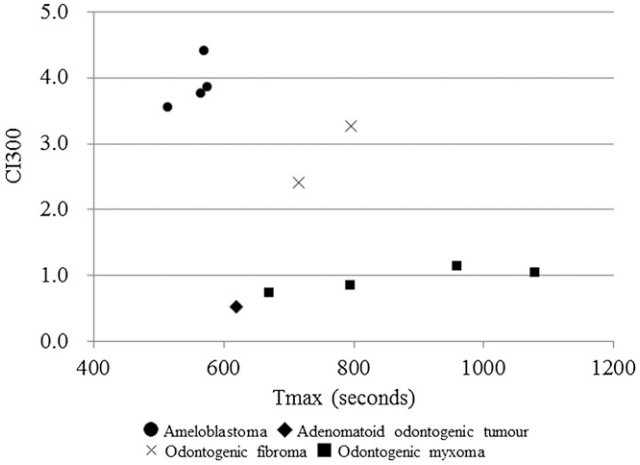

Figure 6 The relationship between the time when the maximum contrast index (CI_{max}) occurred (T_{max}) and the CI_{max} values of the odontogenic tumours in the late enhancement group (T_{max} > 300 s).

sometimes difficult to diagnose with radiographic examinations. On MR images, many odontogenic tumours with soft-tissue components display solid components, while some contain liquid components. The latter tumours, which include KCOTs, AOTs, CCOTs and some ameloblastomas, display a cystic appearance with or without solid components.[1,5,11,12] We evaluated odontogenic tumours on MRI by analysing their cystic component uniformity and DCE-MRI parameters.

KCOT is a cystic lesion with a characteristic parakeratinized stratified squamous epithelial lining. Generally, MRI of KCOTs displays cystic lesions without any solid portions.[11] Ameloblastomas, AOTs and CCOTs display liquid retention on MRI, and ameloblastoma is the common odontogenic tumour.[1–4] In the WHO (2005) classification, ameloblastoma is categorized into the following four histological types: the solid/multicystic type, extraosseous/peripheral type, desmoplastic type and unicystic type.[1] Unicystic ameloblastoma, which presents as a cyst, is morphologically different from the other histological types, which include solid portions.[1] Unicystic ameloblastomas are often devoid of solid components and tend to display a similar appearance to KCOTs on MRI.[12] Regarding the cystic components of ameloblastoma and KCOTs, Minami et al[11] reported that their T_2 relaxation times are useful for differentiating between these two lesions, and Sumi et al[5] reported that the apparent diffusion coefficients of the cystic components of ameloblastomas and KCOTs might be useful for differentiating between them. The cystic components of ameloblastomas usually include serous liquid-containing protein, while those of KCOTs contain desquamated keratin.[1] These differences in the composition of the cystic fluid between ameloblastomas and KCOTs might affect their T_2 relaxation times and apparent diffusion coefficient values.[5,11]

In examinations of odontogenic tumours, our institute used two sequences (T_2WIs and STIR images) with

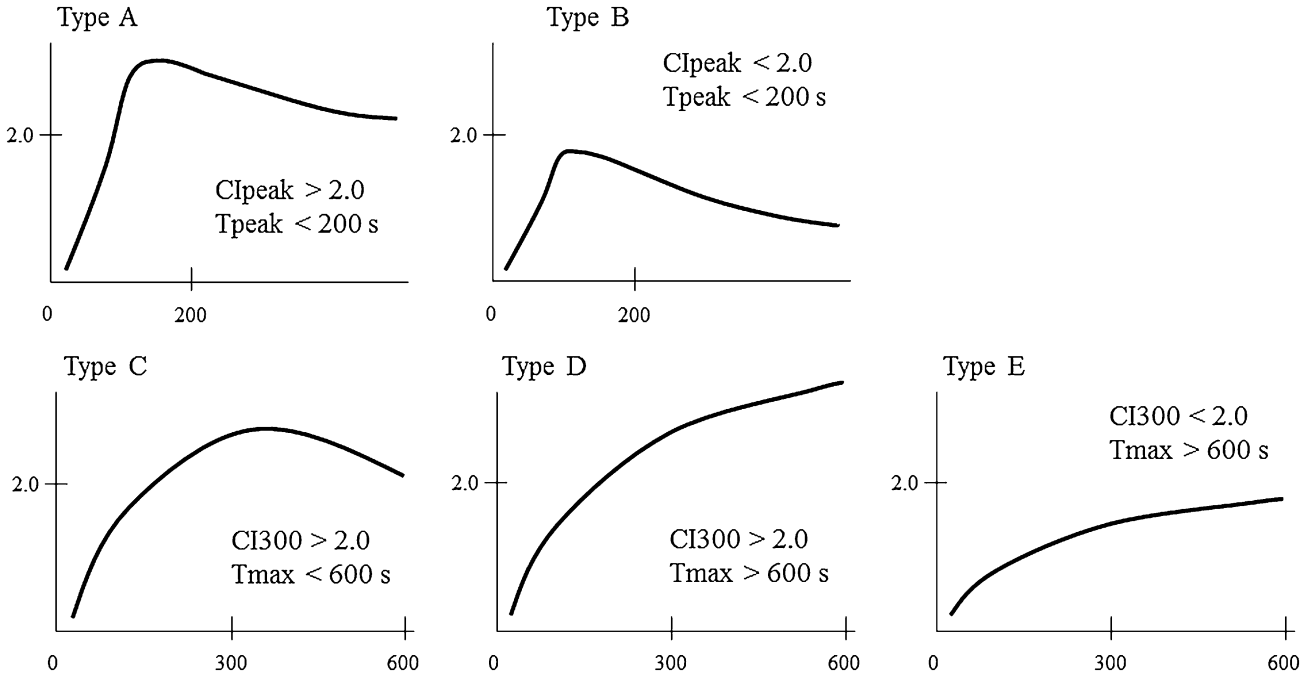

Figure 7 Classification of contrast index (CI) curve patterns. The CI curves were classified into five patterns (Types A–E).

different parameters, but we could not obtain diffusion-weighted images because of the age of our MRI device. Therefore, in this retrospective study, we evaluated the SI uniformity ($U\Sigma$) values of the cystic components of ameloblastomas (including the unicystic type) and KCOTs using the formula devised by the American Association of Physicists in Medicine, which is used in the quality control of MRI. As a result, we found that the cystic components of ameloblastomas and KCOTs displayed significantly different uniformity values on all sequences (T_1WIs, T_2WIs and STIR images). In addition, ROC analysis confirmed that it is possible to differentiate between ameloblastomas and KCOTs using the $U\Sigma$ values of their cystic components on routine sequences, especially T_2WIs (accuracy 100%).

Table 3 Contrast index (CI) curve types among various histopathological diagnosis

	CI curve type				
Histopathological diagnosis	*A*	*B*	*C*	*D*	*E*
Benign					
Ameloblastoma ($n = 16$)	11	1	4	0	0
Odontogenic myxoma ($n = 4$)	0	0	0	0	4
Adenomatoid odontogenic tumour ($n = 3$)	0	2	0	0	1
Odontogenic fibroma ($n = 2$)	0	0	0	2	0
Malignant					
Ameloblastic carcinoma ($n = 1$)	0	1	0	0	0
Primary intraosseous squamous cell carcinoma ($n = 1$)	1	0	0	0	0

CI_{300}, the CI observed at 300 s after contrast medium injection; CI_{peak}, maximum contrast index (CI_{max}) × 0.90; T_{max}, the time when CI_{max} occurred; T_{peak}, the time when CI_{peak} occurred Type A: $CI_{peak} > 2.0$, $T_{peak} < 200$ s; Type B: $CI_{peak} < 2.0$, $T_{peak} > 200$ s; Type C: $CI_{300} > 2.0$, $T_{max} < 600$ s; Type D: $CI_{300} > 2.0$, $T_{max} > 600$ s and Type E: $CI_{300} < 2.0$, $T_{max} > 600$ s.

As for other cystic odontogenic tumours, the cystic components of CCOT should be taken into consideration. This tumour is a benign cystic neoplasm of odontogenic origin that is characterized by an ameloblastoma-like epithelium containing ghost cells, which can become calcified.[1] CCOT-containing calcific substances are relatively easy to distinguish from ameloblastomas, KCOTs and other true jawbone cysts. However, a variable amount of radio-opaque material is seen in about 50% of CCOTs.[1] Thus, to diagnose CCOTs without calcific substances, it might be necessary to compare the uniformity values of CCOTs with those of ameloblastomas and KCOTs. However, we could not evaluate the uniformity values of CCOTs in this retrospective study owing to its rarity (CCOT represents 2.5–7.8% of all odontogenic tumours).[2,3]

For odontogenic tumours with solid components, DCE-MRI, which can analyse the internal structures of lesions, might provide radiologists with useful diagnostic information. Indeed, we have reported the diagnostic value of DCE-MRI and time–SI curves (or CI curves) for jawbone lesions including odontogenic tumours.[6–10] However, although the abovementioned studies were case reports or comparison studies involving one or a few histopathological types, we could not determine how many cases of each histopathological type of odontogenic tumour they examined.[6–10] To the best of our knowledge, there have been no studies of the DCE-MRI parameters of odontogenic tumours. In this

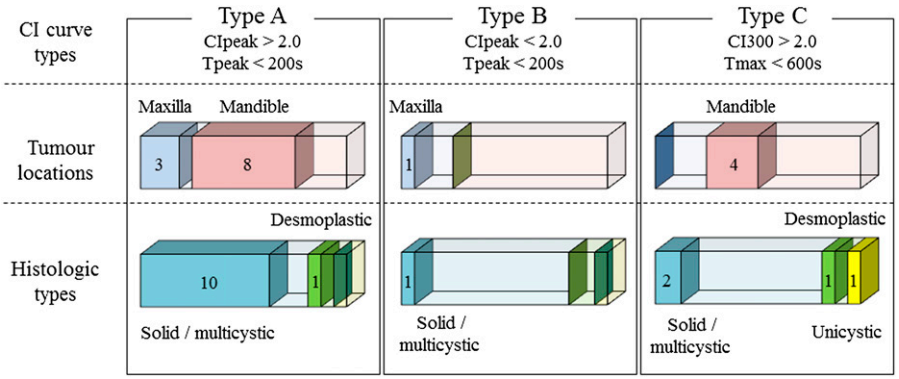

Figure 8 Tumour locations and histological types of ameloblastoma among each contrast index (CI) curve type (Types A–C).

retrospective study of odontogenic tumours, we newly classified odontogenic tumours into five types (Types A–E) on the basis of their DCE-MRI parameters (Figure 8) because the previously developed criteria for head and neck tumours are not appropriate for odontogenic tumours.[14,15]

Odontogenic fibroma and odontogenic myxoma are categorized as neoplasms composed of "mesenchyme and/or odontogenic ectomesenchyme with or without odontogenic epithelium" in the World Health Organization (2005) classification of odontogenic tumours.[1] Odontogenic fibroma is further categorized into the following two histological types: the epithelium-poor type and epithelium-rich type.[1] Our two cases of odontogenic fibroma both belonged to the epithelium-poor type.[9] The main histopathological similarity between odontogenic fibroma and odontogenic myxoma is that they both contain connective tissue with scattered epithelia.[1] Yabuuchi et al[15] reported that the rich fibrous tissue found in the extracellular space of some tumours reduces the washout of contrast medium. According to their theory, the common characteristic of the CI curves of these tumours, *i.e.* the absence of contrast medium washout, agrees with their histopathological features, *i.e.* they contain more rich fibrous tissue than epithelial tissue. The main difference in the CI curves (DCE-MRI parameters) for odontogenic fibroma and odontogenic myxoma was the degree of their enhancement, *i.e.* the odontogenic fibromas displayed higher CI_{600} (*i.e.* the CI observed at 600 s after the contrast medium injection) values than the odontogenic myxomas. The mesenchymal tissue of odontogenic myxoma contains an abundant myxoid or mucoid extracellular matrix, which is not found in odontogenic fibroma.[1] We consider that the presence of extracellular matrix tissue among stromal tissue might influence the inflow of contrast medium into odontogenic myxoma. One of the limitations of our study is that we did not encounter any cases of ameloblastic fibroma, which displays similar histopathological features to odontogenic fibroma.[1]

Ameloblastoma is categorized into four histological types as described previously.[1] Among these four histological types, the ratio of the amount of parenchymal tissue to the amount of stromal tissue varies between desmoplastic ameloblastoma and the other histological types.[1] Similar results might also be obtained for tumours at different locations, *i.e.* differences in blood flow might exist between tumours located in the maxilla and mandible. These differences among each histological type and tumour location could influence a lesion's DCE-MRI parameters. Hence, we considered it necessary to evaluate the relationships between DCE-MRI parameters and histological type or tumour location in ameloblastoma. Approximately 80% of the ameloblastomas belonged to the solid/multicystic type, which is the most common form of ameloblastoma, and 75% of them were located in the mandible. There were no relationships between DCE-MRI parameters and the histological type or tumour location among the ameloblastomas. Although this might have been caused by the small number of subjects, such relationships might vary depending on the histopathological type of ameloblastoma involved.

AOT is a rare odontogenic tumour that accounts for less than 10% of all odontogenic tumours.[1–4] On radiographs, AOTs display a radiolucent cystic appearance, and approximately two-thirds of them include radio-opaque foci.[1] All three of our AOT cases displayed radio-opaque foci. Histopathologically, AOT is composed of odontogenic epithelial tissue arranged in a variety of histoarchitectural patterns and embedded in a mature connective tissue stroma, which sometimes contains hyaline or dysplastic materials.[1] Generally, the mature connective tissue stroma of AOTs is loosely structured, is present in small amounts and contains thin-walled congested vessels.[1] These histopathological features of AOTs are consistent with our findings, *i.e.* the CI curves of two of the three AOT cases were categorized as Type B (tumours of this type display weak enhancement). The remaining AOT (tumour dimensions: $12 \times 8 \times 15$ mm), which was categorized into Type E, was smaller than the Type B AOTs (tumour dimensions: $20 \times 16 \times 29$ mm and $57 \times 28 \times 32$ mm, respectively). We considered that the pathological maturity of the AOT might have affected their CI curve patterns.

Differentiating between benign and malignant tumours is one of the most important issues in the imaging diagnosis of tumours. In this retrospective study, we were only able to evaluate two malignant odontogenic tumours owing to their extreme rarity.[1–4] One subject had primary-type ameloblastic carcinoma, which is a primary odontogenic malignancy that combines the histological features of ameloblastoma with cytological atypia.[1,10] The other subject had solid-type PIOSCC, which is a central jawbone carcinoma arising from odontogenic epithelial remnants.[1,16] Among head and neck lesions, the time–SI curves (or CI curves) of malignant neoplasms commonly display rapid increases followed by rapid decreases.[14,15] However, the CI curves of both our malignant odontogenic tumours displayed similar patterns to those of benign odontogenic tumours, and their DCE-MRI parameters were not useful for their differential diagnosis. Odontogenic tumours arise in the jawbones, while most other head and neck tumours arise from soft tissue. The differences in blood supply to the tumour from the surrounding tissue between odontogenic tumours and other tumours might have been responsible for the results of this study. However, our study included too few subjects to allow us to evaluate this issue.

This retrospective study had the following two limitations: first, we used two types of contrast material, gadopentetate dimeglumine and gadodiamide hydrate, and second, the contrast medium was administered via manual injection. These limitations might have interfered with our results. In addition, some tumours could be diagnosed from their radiographs owing to their typical radiographic appearance, *e.g.* root resorption of the adjacent teeth by the lesion, lesions involving the tooth crown or the presence of disease-specific internal septa, producing a soap-bubble or tennis racket appearance. Furthermore, in the diagnosis of the two malignant odontogenic tumours, the finding that some or all the tumour margin was invasive on radiographic images was a decisive factor in them being diagnosed as malignant.[10,16] On the other hand, DCE-MRI might give us useful information for diagnosing odontogenic tumours when they are still small, and, hence, lack typical radiographic features. The DCE-MRI parameters of tumours that mainly consist of mesenchymal tissue, such as odontogenic fibroma and odontogenic myxoma, displayed particularly characteristic values. This study also suggested that the presence of extracellular matrix tissue among stromal tissue might influence the behaviour of contrast medium, *i.e.* its inflow and washout patterns.

In conclusion, cystic component uniformity was found to be useful for differentiating between ameloblastomas and KCOTs. The DCE-MRI parameters of odontogenic tumours, except for odontogenic fibroma and odontogenic myxoma, contributed little to their differential diagnosis.

References

1. Philipsen HP, Reichart PA, Slootweg PJ, Slater LJ. Neoplasms and tumour-like lesions arising from the odontogenic apparatus and maxillofacial skeleton: introduction. In: Barnes L, Eveson JW, Reichart P, Sidransky D, eds. *Pathology and genetics of head and neck tumours.* Lyon, France: International Agency for Research on Cancer; 2005. pp 283–327.
2. Ochsenius G, Ortega A, Godoy L, Penafiel C, Escobar E. Odontogenic tumors in Chile: a study of 362 cases. *J Oral Pathol Med* 2002; **31**: 415–420.
3. Adebayo ET, Ajike SO, Adekeye EO. A review of 318 odontogenic tumors in Kaduna, Nigeria. *J Oral Maxillofac Surg* 2005; **63**: 811–819.
4. Olgac V, Koseoglu BG, Aksakalli N. Odontogenic tumours in Istanbul: 527 cases. *Br J Oral Maxillofac Surg* 2006; **44**: 386–388.
5. Sumi M, Ichikawa Y, Katayama I, Tashiro S, Nakamura T. Diffusion-weighted MR imaging of ameloblastomas and keratocystic odontogenic tumors: differentiation by apparent diffusion coefficients of cystic lesions. *AJNR Am J Neuroradiol* 2008; **29**: 1897–1901.
6. Asaumi J, Matsuzaki H, Hisatomi M, Konouchi H, Shigehara H, Kishi K. Application of dynamic MRI to differentiating odontogenic myxomas from ameloblastomas. *Eur J Radiol* 2002; **43**: 37–41.
7. Asaumi J, Yanagi Y, Konouchi H, Hisatomi M, Matsuzaki H, Shigehara H, et al. Assessment of MRI and dynamic contrast-enhanced MRI in the differential diagnosis of adenomatoid odontogenic tumor. *Eur J Radiol* 2004; **51**: 252–256.
8. Asaumi J, Hisatomi M, Yanagi Y, Matsuzaki H, Choi YS, Kawai N, et al. Assessment of ameloblastomas using MRI and dynamic contrast-enhanced MRI. *Eur J Radiol* 2005; **56**: 25–30.
9. Hara M, Matsuzaki H, Katase N, Yanagi Y, Unetsubo T, Asaumi J, et al. Central odontogenic fibroma of the jawbone: 2 case reports describing its imaging features and an analysis of its DCE-MRI findings. *Oral Surg Oral Med Oral Pathol Oral Radiol* 2012; **113**: e51–e58.
10. Matsuzaki H, Katase N, Hara M, Asaumi J, Yanagi Y, Unetsubo T, et al. Ameloblastic carcinoma: a case report with radiological features of computed tomography and magnetic resonance imaging and positron emission tomography. *Oral Surg Oral Med Oral Pathol Oral Radiol Endod* 2011; **112**: e40–e47.
11. Minami M, Kaneda T, Ozawa K, Yamamoto H, Itai Y, Ozawa M, et al. Cystic lesions of the maxillomandibular region: MR imaging distinction of odontogenic keratocysts and ameloblastomas from other cysts. *AJR Am J Roentgenol* 1996; **166**: 943–949.
12. Konouchi H, Asaumi J, Yanagi Y, Hisatomi M, Kawai N, Matsuzaki H, et al. Usefulness of contrast enhanced-MRI in the diagnosis of unicystic ameloblastoma. *Oral Oncol* 2006; **42**: 481–486.
13. Price RR, Axel L, Morgan T, Newman R, Perman W, Schneiders N, et al. Quality assurance methods and phantoms for magnetic resonance imaging: report of AAPM nuclear magnetic resonance Task Group No. 1. *Med Phys* 1990; **17**: 287–295.
14. Takashima S, Noguchi Y, Okumura T, Aruga H, Kobayashi T. Dynamic MR imaging in the head and neck. *Radiology* 1993; **189**: 813–821.
15. Yabuuchi H, Fukuya T, Tajima T, Hachitanda Y, Tomita K, Koga M. Salivary gland tumors: diagnostic value of gadolinium-enhanced dynamic MR imaging with histopathologic correlation. *Radiology* 2003; **226**: 345–354.
16. Matsuzaki H, Katase N, Matsumura T, Hara M, Yanagi Y, Nagatsuka H, et al. Solid-type primary intraosseous squamous cell carcinoma of the mandible: a case report with imaging features. *Oral Surg Oral Med Oral Pathol Oral Radiol* 2012; **114**: e71–77.